ELSEVIER

Contents lists available at ScienceDirect

Chemical Geology

journal homepage: www.elsevier.com/locate/chemgeo





Fe K α XANES, Fe K β HERFD XANES and EPMA flank method determinations of the oxidation state of Fe in garnet

Megan Holycross ^{a,b,*}, Elizabeth Cottrell ^b, Jay Ague ^{c,d}, Antonio Lanzirotti ^e, Matthew Newville ^e

- ^a Department of Earth and Atmospheric Sciences, Cornell University, Ithaca, NY 14850, USA
- ^b National Museum of Natural History, Smithsonian Institution, Washington, DC 20560, USA
- ^c Department of Earth and Planetary Sciences, Yale University, New Haven, CT 06520, USA
- ^d Yale Peabody Museum of Natural History, New Haven, CT 06520, USA
- e University of Chicago, Chicago, IL 60637, USA

ARTICLEINFO

Editor: S Aulbach

Keywords: Garnet Oxygen fugacity Redox Spectroscopy

ABSTRACT

The ferric to total iron ratios (Fe³⁺/ Σ Fe) of garnets can be paired with thermodynamic mineral activity models to quantify the oxygen fugacity of garnet-bearing rocks. However, techniques with a high analytical and spatial resolution are necessary to distinguish differences in garnet Fe³⁺/\sumsetmes Fe ratios at the percent level and to accurately measure garnets that are zoned or contain inclusions. We acquired conventional Fe $K\alpha$ and high-resolution energy fluorescence detection (HERFD) Fe $K\beta$ X-ray absorption near edge structure (XANES) spectra and electron microprobe flank method analyses on a suite of 27 peridotitic and eclogitic garnets with Fe³⁺/ Σ Fe ratios previously determined by Mössbauer spectroscopy to evaluate the precision of each technique. We examined variations in the energy and intensity of three XANES spectral features as a function of $Fe^{3+}/\sum Fe$ ratios: 1) the intensity ratio of two-post edge features (I-ratio; Fe Kα only); 2) the energy of the Fe edge at 90% normalized intensity ($E_{0.9}$; Fe K α only) and 3) the pre-edge centroid energy (Fe K α and HERFD Fe K β). In accordance with previous work, we find the energies of garnet pre-edge centroids are relatively insensitive to Fe³⁺/ Σ Fe ratios. The I-ratios of peridotitic and eclogitic garnets are offset from each other at low Fe³⁺/ Σ Fe ratios (<0.13); I-ratio garnet XANES calibrations are composition-specific. The E_{0.9} feature is independent of garnet major element composition in spectra that have been corrected for the effects of self-absorption. We produce two Fe K α garnet XANES calibrations based on variations in the E_{0.9} feature; one calibration with all garnet reference materials included (Fe³⁺/\sumset Fe up to 1.0; "all garnet calibration") and another calibration specific to garnets with low $Fe^{3+}/\sum Fe$ ratios ("low ferric calibration"). $Fe^{3+}/\sum Fe$ ratios calculated from the mean of up to 25 flank method measurements on eight garnet reference materials fall within 4% absolute of a one-to-one correlation with Fe3+/ \sum Fe ratios measured by Mössbauer. The standard error of the mean Fe³⁺/ \sum Fe ratio calculated from flank method approaches the Mössbauer-determined $Fe^{3+}/\sum Fe$ ratio within estimated error (3%) after three analyses. Flank method precision is enhanced at higher beam current; however, the precision of the flank method does not approach the precision of XANES under any microprobe analytical condition tested here. Garnet reference materials detailed here are available by request to the Smithsonian Institution.

1. Introduction

The oxidized to total iron $(Fe^{3+}/\sum Fe)$ ratios of crystalline and amorphous materials can provide information about the system's oxygen fugacity (fO_2) . The mineral garnet (grt) forms a wide range of ferric and ferrous iron-bearing solid solutions and may be important in the petrogenesis of both igneous and metamorphic rocks. Consequently, knowledge of iron oxidation states in garnet provides important

information about the conditions of garnet crystallization in Earth's crust and mantle (e.g., Luth et al., 1990; Gudmundsson and Wood, 1995; Canil and O'Neill, 1996; Woodland and Koch, 2003; Woodland, 2009; Yaxley et al., 2012; Stagno et al., 2015; Miller et al., 2016; Aulbach et al., 2017; Holycross and Cottrell, 2023). Garnet $Fe^{3+}/\sum Fe$ ratios may be characterized using bulk techniques like wet chemistry or Mössbauer spectroscopy, but these approaches cannot resolve variations in $Fe^{3+}/\sum Fe$ ratios that may be present at the scale of individual grains (zoning)

^{*} Corresponding author at: Department of Earth and Atmospheric Sciences, Cornell University, Ithaca, NY 14850, USA. *E-mail address:* holycross@cornell.edu (M. Holycross).

and cannot be used to analyze the $Fe^{3+}/\sum Fe$ ratios of garnets with abundant inclusions. Provided a suite of matrix-matched standards with known $Fe^{3+}/\sum Fe$ ratios, Fe X-ray absorption near edge structure (FeXANES) spectroscopy (e.g., Berry et al., 2010; Dyar et al., 2012) and the flank method for electron microprobe (e.g., Höfer and Brey, 2007) offer alternative means of measuring garnet $Fe^{3+}/\sum Fe$ ratios with both high spatial and analytical resolution.

Here we examine the precision of Fe-XANES and flank method-based calibrations for determining garnet Fe $^{3+}/\sum$ Fe ratios. We develop a new composition-independent Mössbauer-based 'conventional' Fe K α XANES calibration for garnet and explore the capabilities of high energy resolution fluorescence detection (HERFD) Fe K β XANES for garnet applications. We establish a flank method approach for electron probe micro analyzer (EPMA) using these same reference materials. We apply the flank method approach and Fe K α XANES calibrations to measure the Fe $^{3+}/\sum$ Fe ratios of unknown garnets from piston-cylinder experiments and exhumed eclogitic terranes and compare the results. Garnet reference materials detailed here are available for loan through the Smithsonian Institution.

2. Background

2.1. XANES overview

X-ray absorption fine structure (XAFS) spectroscopy probes the electronic and molecular energy states of specific elements, yielding information about element valence as well as coordination and bonding environment (Henderson et al., 2014 and references therein). XAFS spectra can be broadly divided into two regions: the near edge structure (i.e., XANES) region located within 40 eV of the main absorption edge and the extended X-ray absorption fine structure (EXAFS) region at higher energies. The XANES region is more sensitive to transitions in bound energy states, while the EXAFS region records the molecular environment of the element.

Synchrotron XANES measurements utilize energy transitions that occur in the electron shells of atoms that have absorbed an incoming photon, creating an electron hole. The subsequent filling of the electron hole generates X-rays that are emitted at fixed energies that are characteristic of the excited atom. Synchrotron XANES allows for microfocused analysis of materials with detection sensitivities at the parts-permillion level. This is useful for petrologists as it can allow measurement of redox equilibria involving multivalent elements to be made with micrometer spatial resolutions (e.g., Sutton et al., 2020). These microfocused analyses typically measure fluorescent X-rays generated during the absorption process using energy dispersive detectors with a typical energy resolution of ~150 eV. An alternative to conventional fluorescence XANES is HERFD XANES, which measures the intensity of fluorescent X-rays using bent crystal analyzer spectrometers that integrate over a narrow region of the X-ray fluorescence line of interest (Bauer, 2014) with energy resolutions of 1-2 eV. This results in two key advantages compared to conventional XANES: 1) reduced or eliminated fluorescence backgrounds and 2) sharper spectral features in the measured XANES region. Thus, HERFD XANES analysis may facilitate detection of subtle differences in element valence that are not distinguishable with conventional XANES (Bordrage et al., 2011; Sutton et al., 2020). Here we specifically use the term "HERFD XANES" where appropriate; all other references to XANES refer to "conventional XANES". Unless otherwise noted, we use the general term Fe-XANES to describe measurements at the Fe K α edge.

The valence of Fe in in silicate glasses has been widely characterized using Mössbauer-based XAFS/XANES calibrations (e.g., Wilke et al., 2005; Berry et al., 2003; Berry et al., 2018; Cottrell et al., 2009, 2018; Zhang et al., 2016, 2018; Dyar et al., 2016a, 2023). The spectral features of the Fe K pre-edge, occurring about 10 eV before the main edge in the XANES region, are related to the 1s→3d electronic transition. The number, position, and intensity of pre-edge peaks depends on the formal

oxidation state and coordination of Fe (Henderson et al., 2014), such that the area-weighted average energy of component fits to the pre-edge peak(s), or "centroid," can be used to quantify the $Fe^{3+}/\sum Fe$ ratio of the glass (e.g., Wilke et al., 2005).

Fe-XANES has also been used to measure Fe valence in multiple mineral systems including pyroxene, amphibole, olivine, iron oxides and garnet (Bajt et al., 1994; Wilke et al., 2001; Petit et al., 2001; McCanta et al., 2004; Berry et al., 2010; Dyar et al., 2012, 2016b; Steven et al., 2022, 2023; Holycross and Cottrell, 2023). Although XANES spectra measured in minerals are broadly similar to those measured in glasses, the spectral features are typically sharper due to the increased structural ordering in crystalline phases. Additionally, the high degree of polarization of the synchrotron X-ray beam means that mineral anisotropy (when present) often results in orientation-dependent changes in the measured intensity of XANES spectral features.

While empirical calibrations based on shifts in the energy position of the pre-edge centroid provide the most precise measurement of Fe³⁺/ \sum Fe ratios in silicate glasses, this may not be the case in minerals. Previous studies of garnet Fe-XANES by Berry et al. (2010) and Dyar et al. (2012) show the average centroid energy of garnet pre-edges are relatively insensitive to $Fe^{3+}/\sum Fe$ ratio, especially at the $Fe^{3+}/\sum Fe$ ratios relevant for mantle garnets (e.g., $Fe^{3+}/\sum Fe < 0.15$; Woodland and Koch, 2003). The Fe pre-edge in garnet is observed to be composed of multiple superimposed peaks with positions and intensities that vary as a function of Fe valence state and coordination. Dyar et al. (2012) noted that minor variations in garnet pre-edge energies could result from slight differences in garnet crystal structure or composition; from errors introduced by the energy calibration procedure, or from the presence of unresolved component peaks with varying intensities that offset the centroid energy of the observed doublet. Alternately, Berry et al. (2010) suggested the poor relationship between centroid energy and garnet Fe³⁺/\sum_Fe ratios could be the result of difficulties in distinguishing the pre-edge features from spectral background.

Here we test whether the increased resolution of HERFD Fe $K\beta$ XANES yields an improved centroid-based calibration for garnet compared to conventional Fe $K\alpha$ XANES. The $K\beta$ emission was selected for HERFD analyses due to its improved resolution when compared to Fe $K\alpha$. For HERFD XANES collected using Fe $K\beta$, the pre-edge features should show a stronger intensity relative to the main edge in the high-resolution scan. We also examine variations in two conventional Fe $K\alpha$ XANES garnet spectral features, the energy position of the edge at an arbitrary intensity of 0.9 (E_{0.9}) and the calculated intensity ratio of two features in the EXAFS region (I-ratio) (Berry et al., 2010; Dyar et al., 2012), as a function of garnet Fe³⁺/ Σ Fe ratio and major element composition.

2.2. Flank method overview

The flank method (Höfer and Brey, 2007) offers an approach for determining the Fe³⁺/ \sum Fe ratios of minerals and glasses by EPMA. Extended background on the flank method for garnet is detailed in Höfer and Brey (2007) with updated procedures provided in Hezel et al. (2024). We provide a brief overview here: the flank method is derived from the principle that the wavelengths and intensities of garnet Fe L α and Fe L β emission lines depend on the concentration of Fe²⁺ and Fe³⁺ in the garnet as well as its total Fe content. Garnet Fe³⁺/ \sum Fe ratios can be quantified by measuring the intensities (counting) at the energy positions associated with the flanks of the Fe L α and Fe L β lines. Variations in the count ratio, Fe L β /L α , at the flank positions track changes in Fe³⁺/ \sum Fe ratios and \sum Fe. Use of the flank method to characterize the Fe³⁺/ \sum Fe ratios of unknown garnets requires a calibration built with a suite of standards with known Fe³⁺/ \sum Fe ratios; flank method calibrations are specific to each electron microprobe.

3. Samples

Garnets have the general formula $[A]_3[B]_2Si_3O_{12}$, where [A] is a dodecahedral site that typically contains a divalent cation (e.g., Fe^{2+} , Mg^{2+} , Ca^{2+}) and [B] is an octahedral site that typically contains a trivalent cation (e.g., Al^{3+} , Cr^{3+} , Fe^{3+}). The dodecahedral site in mantle garnets (e.g., peridotite xenoliths including garnet websterites, garnet lherzolites, garnet dunites, etc.) is dominated by Mg with subordinate Fe and Ca; they also contain more Cr^{3+} on the octahedral site compared to other types of garnet (Supplement). Eclogitic garnets have higher Ca and Ca a

We formed an Fe-XANES and flank method calibration suite from 27 garnets with Fe^{3+}/\sum Fe ratios previously determined by Mössbauer spectroscopy (Table 1). Nineteen garnets are separates from peridotite xenoliths (Luth et al., 1990; Canil and O'Neill, 1996; Woodland et al., 2002), three garnets are separates from eclogite xenoliths (Luth et al., 1990; Woodland et al., 2002) and five garnets are Fe—Al or Fe—Ca compositional end members that were synthesized in experiments (Woodland and O'Neill, 1993, 1995; Boffa Ballaran and Woodland, 2006). Garnet Fe^{3+}/\sum Fe ratios range from 0.013 to 1.0. Samples of two experimental garnets and all natural garnet specimens were made into polished wafers or thin sections prior to XANES analysis. The remaining three experimental garnets were formatted as powders. Garnet compositional data are provided in the Supplemental Material.

We ran additional tests on two sets of samples that are not part of our garnet calibration suite: 1) garnets from eclogitic xenoliths in the Slave craton with Fe³⁺/\sumethingFe ratios previously determined by Mössbauer (Kopylova et al., 2016) and 2) garnets with unknown Fe³⁺/\sumethingFe ratios from experiments (Holycross and Cottrell, 2022, 2023) and exhumed eclogitic terranes in Syros, Greece (e.g., Okrusch and Brocker, 1990; Seck et al., 1996; Dragovic et al., 2012). The collection coordinates for Syros eclogitic garnets are listed in the Supplement. Eclogitic xenoliths in the Slave craton were used to test our preferred XANES calibration; experimental and exhumed terrane garnets were used to compare flank method and XANES determinations of garnet Fe³⁺/\sumethingFe ratios. Additional information for the samples described here can be found in the original references tabulated in the Supplemental Material.

4. Methods

4.1. Fe-XANES

Fe-XANES spectra were collected over seven sessions at GSECARS beamline 13-ID-E at the Advanced Photon Source (APS) and one session at beamline 4-BM (XFM) at the National Synchrotron Light Source II (NSLS-II). The first derivative of the Fe K-edge spectra of Fe foil was set to 7110.7 in all beam sessions. Fe Kα XANES spectra were collected in all seven sessions at APS. HERFD Fe Kß XANES spectra were collected simultaneously with Ka spectra in one session at APS. Garnet spectra were collected in fluorescence mode and measured using either a Vortex ME4 or Canberra SX7 silicon-drift diode detector arrays coupled to a high-speed digital spectrometer system (Quantum Xpress3). Scans were collected from 7012 to 7356 eV with energy selection achieved using a cryogenically-cooled Si (311) monochromator. The pre-edge region was scanned from -100 to -10 eV (relative to 7112 eV) in 2.5 eV steps, the XANES region from -10 to +35 eV in 0.1 eV steps, and the EXAFS region from 3.03 to 8.1 inverse angstroms in 0.05 inverse angstrom steps. A 1 s dwell time was used for all steps. Garnets were analyzed using a focused $2 \times 2 \, \mu m$ spot at APS and a $9 \times 10 \, \mu m$ spot at NSLS-II. Kapton film (~75 µm thickness) was placed before the detector to cut down on Ca fluorescence during analysis and layers of Al foil (typically 100 µm total) were placed upstream of the incident beam to decrease incident flux and

Table 1 Garnet reference materials included in Fe K α XANES calibrations. Garnet reference materials are available for loan from the National Museum of Natural History, Smithsonian Institution.

#	sample name	reference	sample type	format	NMNH catalog number	
		Luth et al.,		garnet		
1	HRV247A	1990	eclogite	wafer	118524-5	
		Luth et al.,		garnet		
2	DE15	1990	eclogite	wafer	118520–1	
	EDDOOO	Luth et al.,	garnet	garnet	110504.0	
3	FRB838	1990 Canil and	lherzolite sp-grt	wafer thin	118524–2	
4	FRB1350	O'Neill, 1996	lherzolite	section	118524-4	
		Canil and	garnet	garnet		
5	FRB921	O'Neill, 1996	websterite	wafer	118524-3	
		Luth et al.,	garnet	garnet		
6	PHN1917	1990	lherzolite	wafer	118518–7	
7	UV417/89	Canil and O'Neill, 1996	garnet lherzolite	garnet wafer	118522-1	
/	0 1417/69	Canil and	merzonte	garnet	116322-1	
8	UV465/86	O'Neill, 1996	garnet dunite	wafer	118522-2	
		Luth et al.,	garnet	garnet		
9	FRB131	1990	lherzolite	wafer	118518-2	
		Luth et al.,	garnet	garnet		
10	PHN5549	1990	lherzolite	wafer	118520–2	
11	FRB135	Luth et al., 1990	garnet lherzolite	garnet wafer	118518-3	
11	PRDISS	Canil and	garnet	garnet	110310-3	
12	F865	O'Neill, 1996	harzburgite	wafer	118524-1	
		Luth et al.,	garnet	garnet		
13	FRB140	1990	lherzolite	wafer	118518-4	
		Luth et al.,	garnet	garnet		
14	BD2501	1990	lherzolite	wafer	118518–1	
15	PHN1925	Luth et al., 1990	garnet lherzolite	garnet wafer	118518-8	
10	111111320	Canil and	garnet	garnet	110010 0	
16	PHN5239	O'Neill, 1996	lherzolite	wafer	118524-6	
		Luth et al.,	garnet	garnet		
17	PHN1503C	1990	megacryst	wafer	118518-5	
10	DIDI1611	Luth et al.,	garnet	garnet	110510 6	
18	PHN1611	1990 Canil and	lherzolite garnet	wafer garnet	118518–6	
19	PHN5267	O'Neill, 1996	lherzolite	wafer	118524-7	
		of individual grts				
	#1-19	Ü		1" round	118530	
		Woodland	garnet	garnet		
20	E1	et al., 2002	lherzolite	wafer	118544	
21	E2	Woodland et al., 2002	aalaaita	garnet wafer	118545	
21	EZ	Woodland	eclogite garnet	garnet	110343	
22	L78	et al., 2002	lherzolite	wafer	118546	
		Woodland and				
23	UHP666a	O'Neill, 1995	experimental	powdered	118543	
		Boffa Ballaran				
		and				
24	PC287b	Woodland, 2006	experimental	powdered	118542	
24	1 0207 0	Boffa Ballaran	experimentar	powdered	110342	
		and				
		Woodland,				
25	PC288a	2006	experimental	powdered	118541	
		of individual grts		1"	110510	
	#20–25	Woodland and		1" round	118540	
26	aw14	Woodland and O'Neill, 1993	experimental	garnet wafer	118547	
20	awi7	Woodland and	capermiental	garnet	11034/	
27	AW52a	O'Neill, 1995	experimental	wafer	118549	

Please request samples by their NMNH catalog number and refer to these catalog numbers in future references. In addition, two mounts with multiple reference materials have been prepared and can be requested via the mount's catalog number. Garnet compositions are presented in the Supplement.

minimize detector dead time at the APS. Typical photon flux densities during garnet analysis were $\sim 3 \times 10^9$ ph/s/ μ m².

HERFD Fe Kβ data were collected at 13-ID-E by measuring the Fe Kβ emission with an energy resolution comparable to the natural energy width of the Fe K level (\sim 1.25 eV). Three high-quality Ge(620) crystals, each 100 mm in diameter and placed on 1-m radius Rowland circles, were aligned to diffract the Fe Kβ1 energy (7059 eV) emission at an angle of 79.0 degrees onto a Dectris Eiger 500 K pixel area detector. A scan of analyzed energy at Fe Kβ1 showed a peak centered at 7059 eV and a full-width-at-half-maximum of 4 eV. A helium-filled environment was used for the flight path from sample to analyzer and analyzer to detector to reduce attenuation of the emitted X-rays. Shielding and a small region of interest (ROI) on the detector into which the emission selected by each analyzer was directed were used to reduce background levels far below the signal level, and the integrated intensity of this selected ROI was used as the HERFD Fe Kβ intensity. By selecting a very narrow energy window at the Fe Kβ1 energy, HERFD XANES gives finer energy resolution of the XANES features and suppresses background fluorescence which can dramatically increase the sensitivity to elements with overlapping lines (Sutton et al., 2022). However, the small solid angle of detection from the three analyzer crystals reduces the fluorescence count rate compared to the conventional energy dispersive fluorescence XANES. We tested whether this trade-off between energy resolution and count rate alters the precision of XANES calibrations based on the centroid energy of the Fe pre-edge peaks.

A minimum of three conventional Fe Kα spectra were recorded on each garnet in all beam sessions, with as many as 24 conventional Fe $K\alpha$ and HERFD Fe Kβ spectra collected on each garnet in a single beam session. Two garnets were repeatedly analyzed to monitor for possible changes in collection conditions (such as changes in the characteristics of the photon source, optics, focusing, foil calibration, thermal load on the monochromator, etc.) that may possibly have led to change in the energy of the incident X-ray beam (i.e., "energy drift") throughout the course of each beam session. This also allows for high precision energy calibration between sessions and facilities. Garnet F865 was analyzed every 2-3 h across seven sessions; garnet UV417-89 was used as the internal standard instead of F865 in one session. Monochromator drift between sessions was accounted for by correcting spectra to the average value of the E_{0.9} feature (see Results) of garnet F865 collected in APS2019–1; F865 \equiv 7121.60 eV. Similarly, the drift between sessions in APS2020–3 was accounted for by correcting spectra to the average value of the $E_{0.9}$ feature of UV417–89 collected in APS2019–1; UV417–89 \equiv 7121.57 eV. Garnet I-ratios were corrected between sessions to the set value of garnet F865 \equiv 1.31. Garnet centroids were calculated using data collected in only one session and therefore the absolute values were not normalized between sessions. We did not observe any systematic time-dependent changes to the spectra within a single session; accordingly, no time-dependent corrections were applied to spectra collected within a single session.

We assessed the potential for the high-energy photon beam to cause changes to the spectra ("beam damage") by varying the photon dose according to established methods (Cottrell et al., 2018). We did not observe any dose-dependent spectral changes.

The crystallographic orientations of measured garnets are unknown. Garnet has an isometric (cubic) structure; no spectral orientation effects are anticipated for crystals in this system. Multiple randomly oriented garnet grains from the same sample show identical spectral features, confirming the orientation independence of our garnet XANES calibrations.

All garnet spectra were processed in XAS Viewer, provided as part of the Larch software package (Newville, 2013). Spectra were corrected for detector deadtime and normalized to the average absorption coefficient (edge-step) in the region 7200–7350 eV. All spectra were corrected for the effect of Fe over-absorption in XAS Viewer using garnet major element stoichiometry. Garnets were corrected using stoichiometric formulas including only values for Si, Al, Mg, Ca, total Fe and O to the

first decimal place (e.g., Fe_{0.6}Mg_{2.2}Ca_{0.4}Al_{1.8}Si_{3.0}O₁₂ [Supplement]).

Garnet Fe-XANES spectra were reduced using three different techniques: 1) the I-ratio, the calculation of the ratio of the intensities of two spectral features near the post-edge; 2) the $E_{0.9}$ method, the calculation of the energy of the main absorption edge at an arbitrary intensity of 0.9; 3) calculation of the area-weighted pre-edge centroid. The first two reduction methodologies were applied only to the conventional Fe Kα garnet spectra. Area-weighted centroids were calculated for conventional Fe K α and HERFD Fe K β pre-edges collected in the same beam session. Pre-edge centroids were calculated in XAS Viewer using the following method: the fit energy range was set to 7106-7117; the background was fit with a linear + Lorentzian form for the main Fe K edge, and two Lorentzian peak components were fit to each multiplet in the pre-edge. Multiple fits to the pre-edge region of a single spectrum yielded centroids that varied by less than the standard error of the fit as calculated by XAS Viewer (Table 2). However, we note that the standard errors of our garnet centroid fits are significantly larger than the typical precision of centroid-based Fe-XANES calibrations for silicate glasses (up to \sim 0.04 eV for garnet compared to 0.008 \pm 0.005 eV for glasses; e. g., Cottrell et al., 2009).

4.2. Flank method

Flank method analyses were performed on the JEOL 8530F Field Emission electron microprobe at the National Museum of Natural History, Smithsonian Institution, following the methodologies of Höfer and Brey (2007) and Tao et al. (2018). Spectrometer calibration was executed on an iron metal standard at 25 kV and 80 nA using a TAP crystal with the slit on the spectrometer set at 300 μm . The Fe K α 9th order line was scanned to verify the measurement positions for the flank method following the procedure of Höfer et al., 2000. Count intensities were determined at each measurement position, normalized to beam current and plotted versus spectrometer shift position. The difference between the theoretical position of the Fe Ka 9th order peak (189.417 mm) and the measured peak position on the NMNH microprobe was used to calculate the positions of the Fe L α and L β peaks for the chosen analytical conditions. The two positions were entered in our analytical routine as "dummy" elements As and Br, respectively, with counting times of 300 s. Silicon, Al, Mg, Mn, Ca, Na, K, and Ti were included in the same analytical routine with counting times of 60 s. Details of the flank method set up are included in the Supplement.

We tested two different beam conditions for flank method measurements: 15 kV and 60 nA, and 15 kV and 80 nA. The 60 nA calibration was built from eight garnet reference materials with Mössbauer-determined Fe³⁺/ Σ Fe ratios from 0.01 to 0.70. We analyzed 25 points on all garnets using a 5 \times 5 grid and calculated the L β /L α ratio (cps "Br"/ cps "Ar") at each point. We plotted the average $L\beta/L\alpha$ ratio for each garnet vs. the average Fe²⁺ (wt%) value of each garnet (as calculated from the EPMA analyses of FeO and Mössbauer analyses of Fe $^{3+}/\sum$ Fe ratios). The linear relationship between the two values represents the self-absorption effect caused by varying Fe concentration (Höfer and Brey, 2007). The $L\beta/L\alpha$ ratio of a garnet with unknown Fe^{3+} will deviate from this linear relationship by a "delta" value (Δ value = the offset between the measured $L\beta/L\alpha$ ratio and the theoretical $L\beta/L\alpha$ ratio if all iron was present as Fe²⁺), enabling measurement of the garnet Fe³⁺ content. The Δ value for each garnet reference material was calculated from a trend line fit to the plot of garnet Fe^{2+} vs $L\beta/L\alpha$ ratio. Average Δ values were calculated and plotted against the average Fe3+ (wt%) value of each garnet (as calculated from the EPMA analyses of FeO and Mössbauer analyses of $Fe^{3+}/\sum Fe$ ratios). The trendline fit to this data was used to calculate the Fe³⁺ values of unknown garnets from measured Δ values. See the Supplement for measurement details.

Six garnet reference materials with Mössbauer-determined Fe $^{3+}$ / Σ Fe ratios from 0.02 to 0.11 were measured at 80 nA to determine if higher count rates resulting from increased beam current yield a better-resolved flank method calibration. Two of the six garnets were measured

Name	Fe ³⁺ /∑Fe (Mössbauer)	Estimated SE	mean I- ratio	I-ratio SD	n (I ratio)	Mean E _{0.9}	E _{0.9} SD	n (E _{0.9})	Kβ HERFD centroid	Centroid fit SE	n (centroid)	Kα centroid	Centroid SD	n (centroid)
aw14	0.01	0.03	1.41	0.013	5	7121.47	0.07	9	7111.67	0.02	1	7111.94	0.02	7
HRV247A	0.02	0.03	1.32	0.007	3	7121.46	0.02	20	7111.71	0.03	1	7112.00	0.02	15
DE15	0.02	0.03	1.29	0.010	3	7121.51	0.03	26						
FRB 838	0.03	0.03	1.34	0.007	3	7121.54	0.03	7	7111.84	0.04	1	7111.92	0.08	13
FRB1350	0.04	0.03	1.37	0.001	3	7121.47	0.01	3						
FRB921	0.05	0.03	1.33	0.005	3	7121.56	0.03	3						
PHN1917	0.05	0.03	1.34	0.002	3	7121.53	0.02	5						
UV417/89	0.05	0.03	1.33	0.002	3	7121.57	0.03	32						
UV465/86	0.05	0.03	1.34	0.002	3	7121.56	0.01	3						
FRB131	0.05	0.03	1.33	0.004	3	7121.59	0.04	16	7111.73	0.03	1	7112.00	0.02	13
PHN5549	0.05	0.03	1.31	0.003	3	7121.62	0.01	10	7111.67	0.06	1	7111.98	0.01	7
FRB135	0.06	0.03	1.32	0.004	3	7121.56	0.01	3						
E2	0.06	0.03	1.28	0.004	3	7121.56	0.03	16	7111.79	0.05	1	7112.16	0.03	10
L78	0.07	0.03	1.28	0.005	3	7121.68	0.02	6						
F865	0.08	0.03	1.31	0.006	34	7121.60	0.04	63	7111.83	0.03	1	7112.08	0.07	10
E1	0.09	0.03	1.25	0.006	3	7121.73	0.02	28						
FRB140	0.11	0.03	1.26	0.003	3	7121.70	0.01	3						
BD2501	0.11	0.03	1.26	0.002	3	7121.76	0.04	14	7112.03	0.08	1	7112.24	0.02	9
PHN1925	0.12	0.03	1.24	0.001	3	7121.73	0.00	9	7111.95	0.06	1	7112.16	0.01	9
PHN5239	0.12	0.03	1.25	0.004	9	7121.70	0.01	9						
PHN 1503C	0.12	0.03	1.25	0.001	3	7121.72	0.02	19	7111.70	0.04	1	7112.45	0.03	16
PHN1611	0.12	0.03	1.26	0.000	3	7121.75	0.02	24	7112.03	0.05	1	7112.16	0.02	24
PHN5267	0.13	0.03	1.26	0.001	3	7121.78	0.02	14	7111.93	0.10	1	7112.20	0.01	9
UHP666	0.46	0.03	0.86	0.039	4	7122.87	0.06	4						
AW52a	0.70	0.03	0.73	0.003	5	7124.34	0.22	12	7112.43	0.03	1	7113.20	0.01	4
PC287b	1.00	0.03	0.69	0.012	4	7126.68	0.20	3						
PC288a	1.00	0.03	0.59	0.020	4	7126.78	0.14	3						

in 5×5 grids (25 points total). The other four garnets were measured at 80 nA for n=4 or 5 points (Supplement). All garnets with unknown Fe³⁺/ Σ Fe ratios were measured at 80 nA.

5. Results

5.1. Garnet Fe-XANES

Garnet XANES spectra exhibit systematic differences in energy and intensity as a function of garnet $Fe^{3+}/\Sigma Fe$ ratios. We investigated variations in three Fe-XANES spectral features that could be used to build an empirical calibration to characterize the $Fe^{3+}/\Sigma Fe$ ratios of garnet unknowns. We examined the relationships between Mössbauer-determined $Fe^{3+}/\Sigma Fe$ ratios of our garnet standards and the ratio of the intensities of post-edge features at 7138.4 and 7161.7 eV (I-ratios; 27 garnets); the position of the absorption edge energy at a normalized intensity of 0.9 (E_{0.9}; 27 garnets), and the centroids of Fe K α and HERFD Fe K β pre-edges (13 garnets). We are particularly interested in examining the spectral features of garnets with low $Fe^{3+}/\Sigma Fe$ ratios ($Fe^{3+}/\Sigma Fe \leq 0.13$) that are most representative of natural peridotitic and eclogitic compositions.

Berry et al. (2010) found the Fe³⁺/ Σ Fe ratios of mantle garnets could be distinguished with high accuracy and precision by the ratio of the intensities of two features in the EXAFS region ("I-ratio"). However, Dvar et al. (2012) determined that over a broader compositional range, parameterizations based on garnet I-ratios yielded poorer correlations than other methods they tested. Here we evaluate the sensitivity of the Iratio parameter to garnet $Fe^{3+}/\Sigma Fe$ ratios in samples of varying composition. We define the I-ratio as the intensity of the post-edge feature at 7162.95 divided by the intensity of the feature at 7139.65 eV. Our I-ratio numerator and denominator are shifted relative to the values used by Berry et al. (2010) to account for differences in monochromator calibration at APS and NSLSII. I-ratio values for all garnets are shown in Table 2. The I-ratios of all garnet reference materials form a coherent array when plotted against their $Fe^{3+}/\Sigma Fe$ ratios that is best fit by a polynomial with $R^2 = 0.98$, n = 27 (Fig. 1a and Supplemental Material). The coherence of the trend holds for garnets with peridotitic compositions when only garnets with $Fe^{3+}/\Sigma Fe$ ratios ≤ 0.13 are considered (Fig. 1b). At low Fe³⁺/ Σ Fe ratios, the relationship between peridotitic garnet I-ratios and $\mathrm{Fe^{3+}/\Sigma Fe}$ values is best fit by a linear regression. A leave-one-out statistical analysis (e.g., Arlot and Celisse, 2010) of our I-ratio garnet calibration for low ferric peridotitic compositions indicates an uncertainty in Fe³⁺/ Σ Fe ratio = 0.02 (1 σ) (Table 3). The I-ratios of eclogitic garnets are offset from the peridotitic calibration by $Fe^{3+}/\Sigma Fe = 0.03$ to 0.06. This offset is greater than or equal to the estimated error on the Mössbauer analyses of ± 0.03 and greater than the uncertainty on the low ferric peridotite-only I-ratio calibration.

The precision of the I-ratio technique is enhanced if the calibration suite is limited to high-Mg, low-Ca garnets (i.e., peridotitic garnets). If the eclogitic garnets are included in an I-ratio calibration with all garnets with $Fe^{3+}/\Sigma Fe$ ratios $\leq\!0.13$, a leave-one-out statistical analysis shows the uncertainty of the calibration increases to 0.05 (1 σ). This implies low-Mg, high-Ca eclogitic garnets require their own I-ratio calibration. While the shift in I-ratios for compositionally similar garnets may primarily reflect an increasing proportion of Fe^{3+} on the garnet octahedral site (e.g., Berry et al., 2010), the calibration offset for the eclogitic compositions suggests the post-edge structures of garnet spectra are sensitive to other parameters in addition to $Fe^{3+}/\Sigma Fe$ ratios.

XANES analyses of many garnets of different composition and constant $Fe^{3+}/\Sigma Fe$ ratios are needed to systematically investigate the cause of variations in garnet post-edge structure. Our standard suite contains four garnets with average $Fe^{3+}/\Sigma Fe=0.054$ and two garnets each with $Fe^{3+}/\Sigma Fe=0.048$ and 0.122 (all values are as reported in the original Mössbauer spectroscopy publications). Eclogitic garnets contain more Ca and Fe and less Mg and Cr compared to peridotitic garnets, raising the possibility that the offset between calculated I-ratios in each suite could be due to garnet composition. We examined correlations between garnet

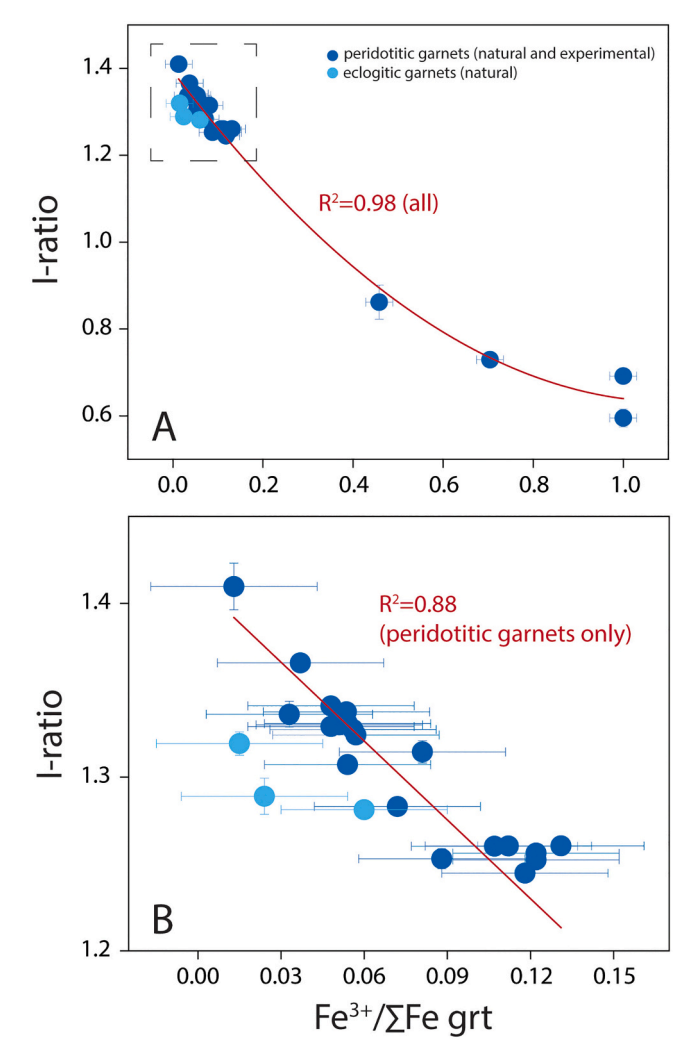


Fig. 1. A. The intensity ratios (I-ratios) of Fe-XANES post-edge features at 7162.95/7139.65 eV compared to Mössbauer measurements of Fe³⁺/ Σ Fe ratios for all garnets in Table 1. The relationship between I-ratio and garnet Fe³⁺/ Σ Fe ratio (Fe³⁺/ Σ Fe up to 1.0) is best fit by a second-order polynomial with R² = 0.98. All garnet compositions (peridotitic and eclogitic) are included in the fit. Dashed box shows region of interest for Fig. 3b. B. I-ratios vs. garnet $Fe^{3+}/\Sigma Fe$ ratios for samples with ${\rm Fe^{3+}/\Sigma Fe} \le 0.13$. The linear relationship between I-ratio and $Fe^{3+}/\Sigma Fe$ ratio for peridotitic garnets (red line) has an R^2 value of 0.88. The I-ratios of eclogitic garnets are offset from the peridotitic garnet relationship, indicating the I-ratio feature may be sensitive to major element composition as well as $Fe^{3+}/\Sigma Fe$ ratio. Vertical error bars are the standard deviations of multiple measurements on the same garnet; standard deviations are smaller than the symbol where not pictured. Horizontal error bars represent estimated Mössbauer spectroscopy errors of \pm 3% Fe³⁺/ Σ Fe. Figure modified from Holycross and Cottrell (2023). (For interpretation of the references to colour in this figure legend, the reader is referred to the web version of this article.)

compositional parameters and calculated I-ratios at constant Fe $^{3+}/\Sigma Fe$ ratio. We find a systematic positive relationship between garnet I-ratios and Cr_2O_3 concentration at constant $Fe^{3+}/\Sigma Fe$ for all groups (Fig. 2). The I-ratios of two garnets in our suite with $Fe^{3+}/\Sigma Fe=1$ are also offset from one another; these garnets do not contain Cr_2O_3 but have varying CaO contents. However, there is no correlation between CaO and I-ratios across all groups at constant $Fe^{3+}/\Sigma Fe$ (see data in Supplement). The apparent relationship between garnet I-ratios and Cr_2O_3 concentrations is constructed from few data points, and additional data are needed to assess what factors cause the eclogitic garnets to deviate from the peridotitic garnet calibration. Because features in the post-edge region are the result of multiple scattering processes (e.g., Farges et al., 1996),

Table 3 Regression coefficients for reported Fe K α XANES calibrations. Coefficients are presented with 1σ uncertainties in parentheses. Calibration uncertainties are 1σ .

		Coefficients		Calibration uncertainty ($\pm \mathrm{Fe}^{3+}/$	
Calibration	Equation form	a	a b		
E _{0.9} , low ferric	Fe ³⁺ / \sum Fe = a + b*[E _{0.9} -7121.6] Fe ³⁺ / \sum Fe = a + b*[E _{0.9} -7121.6] + c*	0.0652 (0.0026) 0.0664	0.3464 (0.0260)	-0.0262	0.02
E _{0.9} , all I-ratio, low ferric	$[E_{0.9}-7121.6]^2$	(0.0032) 0.0705	0.3158 (0.0096) -0.7263	(0.0020)	0.04
peridotite	$Fe^{3+}/\sum Fe = a + b*[I \text{ ratio - 1.31}]$	(0.0030)	(0.0646)		0.02

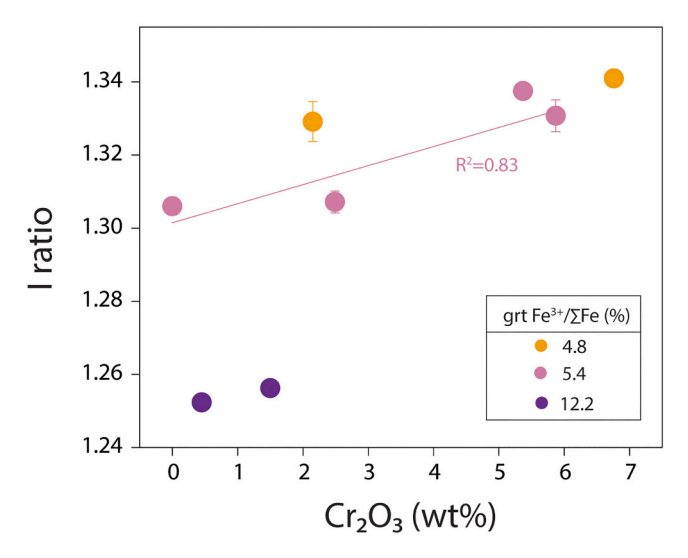


Fig. 2. The I-ratios of garnets with constant $Fe^{3+}/\Sigma Fe$ ratio increase as Cr_2O_3 concentration increases. The correlation between I-ratio and Cr_2O_3 content for garnets with $Fe^{3+}/\Sigma Fe = 0.054$ (pink line) has an R^2 value of 0.83. (For interpretation of the references to colour in this figure legend, the reader is referred to the web version of this article.)

variations in garnet I-ratios may not have a straightforward interpretation and could derive from changes in more than one compositional or structural parameter.

Berry et al. (2003, 2010) and Dyar et al. (2012) demonstrated the energy of the main absorption edge at an arbitrary intensity of 0.9 (E_{0.9}) is sensitive to changing Fe³⁺/ Σ Fe ratios in isotropic materials. Berry et al. (2010) found there were offsets in the edge energies of two populations of garnet in spectra that had not been corrected for the effects of over-absorption. The degree of over-absorption increases with Fe content. Left uncorrected, over-absorption will attenuate the intensity of the edge and result in an apparent shift of the normalized edge to lower energy (Iida and Noma, 1993; Berry et al., 2010). This leads to calculated garnet Fe³⁺/ Σ Fe ratios that are lower than "true" using the E_{0.9} method.

We applied an over-absorption correction to all spectra in the XAS Viewer software using the major element stoichiometry of measured garnets. An over-absorption correction is critical for accurate employment of the $E_{0.9}$ parameterization (Holycross and Cottrell, 2023). In contrast to the I-ratio method, the relationship between $E_{0.9}$ and the $Fe^{3+}/\Sigma Fe$ ratios of the measured garnets defines a coherent array for all compositions at all $Fe^{3+}/\Sigma Fe$ ratios (Table 2; Fig. 3). Dyar et al. (2012) also noted that compared to the I-ratio technique, the $E_{0.9}$ method yields a better correlation with garnet $Fe^{3+}/\Sigma Fe$ ratios in spectra that have been corrected for the effects of over-absorption. The relationship between the $E_{0.9}$ parameter and garnet $Fe^{3+}/\Sigma Fe$ ratios of all reference materials (i.e., $Fe^{3+}/\Sigma Fe=0.013-1$) is best fit by a polynomial equation (Table 3; Fig. 3a) with an $R^2=0.99,\,n=27$ (Supplement and Holycross and Cottrell, 2023). A leave-one-out cross validation analysis indicates

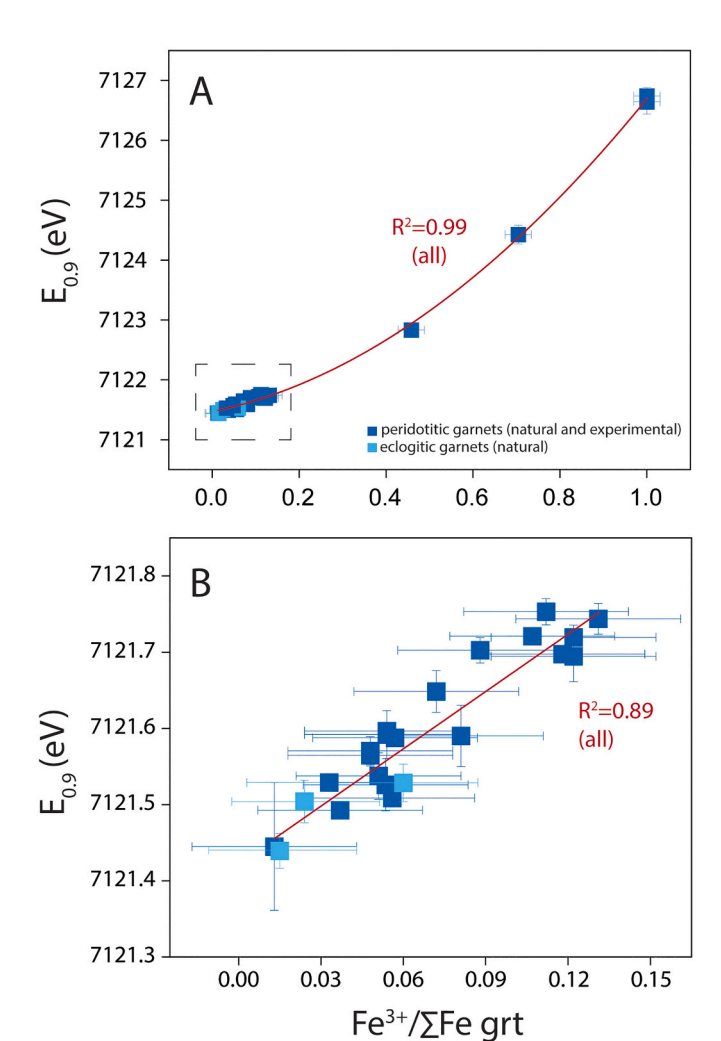


Fig. 3. A. The energy position of the Fe-edge at 90% normalized intensity $(E_{0.9})$ compared to Mössbauer measurements of $\mathrm{Fe^{3+}/\Sigma Fe}$ ratios for all garnets in Table 1. The relationship between $E_{0.9}$ values and garnet $\mathrm{Fe^{3+}/\Sigma Fe}$ ratio $(\mathrm{Fe^{3+}/\Sigma Fe}$ up to 1.0) is best fit by a second-order polynomial with $R^2=0.99$. All garnet compositions are included in the fit. B. $E_{0.9}$ values vs. garnet $\mathrm{Fe^{3+}/\Sigma Fe}$ ratios for samples with $\mathrm{Fe^{3+}/\Sigma Fe}$ ratio (all compositions) has an R^2 value of 0.89. The $E_{0.9}$ feature is not dependent on garnet composition in spectra that have been corrected for the effects of self-absorption. Vertical errors are the standard deviations of multiple measurements on the same garnet taken over seven beam sessions (up to 63 measurements on a single garnet across all sessions). Horizontal error bars represent estimated Mössbauer spectroscopy errors of \pm 3% $\mathrm{Fe^{3+}/\Sigma Fe}$. Figure modified from Holycross and Cottrell (2023).

the uncertainty on calculated $Fe^{3+}/\Sigma Fe$ ratios for the $E_{0.9}$ calibration including all garnet reference materials is ± 0.04 . We found that an $E_{0.9}$ calibration parameterized with data from garnets with $Fe^{3+}/\Sigma Fe$

ratios \leq 0.13 ("low ferric calibration") better reproduces the values of the garnet reference materials over the same Fe^3+/\$\Sigma Fe\$ range compared to an E_{0.9} calibration parameterized with data from all garnets (e.g., with Fe³+/\$\Sigma Fe\$ up to 1) (Supplemental Material and Holycross and Cottrell, 2023). A linear regression for the low ferric calibration (Table 3, Fig. 3a) has R² = 0.89, n = 23. A leave-one-out cross validation shows the 1\$\sigma\$ uncertainty for garnet Fe³+/\$\Sigma Fe\$ ratios with using this calibration is \$\pm 0.02\$ (Holycross and Cottrell, 2023). Calibrations relating E_{0.9} to garnet Fe³+/\$\Sigma Fe\$ ratios are tabulated in Table 3, with more expansive statistical analysis provided in the Supplement.

Finally, we investigated variations in the area-weighted centroids of select conventional Fe K α and HERFD Fe K β pre-edges as a function of garnet $Fe^{3+}/\Sigma Fe$ ratios. Berry et al. (2010) and Dyar et al. (2012) demonstrated the average centroid energy of the Fe Kα XANES pre-edges exhibits little variation at garnet Fe³⁺/ Σ Fe ratios<0.2, the critical range for mantle garnets. The poor correlation between Fe Kα XANES centroids and garnet $Fe^{3+}/\Sigma Fe$ ratios was previously interpreted to result from difficulties in distinguishing the low-intensity garnet pre-edges from spectral background (Berry et al., 2010); from variations in garnet structure or composition; from errors in the energy calibration procedure; or from the presence of unresolved component peaks under the preedge (Dyar et al., 2012). The energy resolution of HERFD XANES is typically higher than what can be achieved with conventional XANES, resulting in sharper spectral features and lower backgrounds from the main edge (e.g., Glatzel et al., 2009; Bauer, 2014). Even though the HERFD at Fe Kβ energy collects much less of the Fe fluorescence (both by solid angle and by energy selection) than conventional Fe XANES, this method offers the possibility that garnet HERFD Fe-XANES may improve the precision for pre-edge centroid calibrations and so better distinguish garnet Fe³⁺/ Σ Fe ratios compared to conventional Fe-XANES.

We analyzed a subset of garnets using HERFD Fe K β XANES. Multiple spectra (up to 24) were taken on each garnet composition; spectra for each composition were subsequently merged in XAS Viewer to reduce noise. An example of multiple merged HERFD Fe K β spectra is compared to a single conventional Fe K α spectrum from the same garnet in Fig. 4 The merged HERFD Fe K β spectrum is significantly noisier than the Fe K α spectrum due to the low solid-angle of detection, though the spectral background is notably lower below the pre-edge peaks (inset image, Fig. 4). HERFD Fe K β main edges appear jagged in close-up and do not form a continuous line, rendering the HERFD K β spectra less precise for application of the E $_{0.9}$ method.

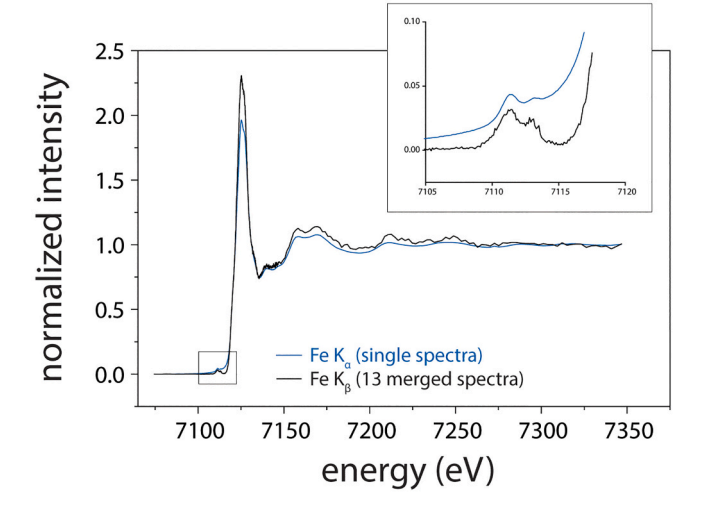


Fig. 4. Thirteen merged HERFD Fe $K\beta$ spectra (black) compared to a single conventional Fe $K\alpha$ spectrum (blue) collected from garnet FRB131. The inset box shows an enlarged view of the pre-edge region. (For interpretation of the references to colour in this figure legend, the reader is referred to the web version of this article.)

Calculated HERFD Fe KB centroids are shown as a function of garnet ${\rm Fe^{3+}/\Sigma Fe}$ ratios for samples with ${\rm Fe^{3+}/\Sigma Fe} \le 0.13$ in Fig. 5a. The correlation between calculated centroids and $Fe^{3+}/\Sigma Fe$ ratios is poor compared to the I-ratio and E_{0.9} calibrations (a linear regression through all data has an $R^2 = 0.44$), perhaps in part due to difficulties accurately fitting the noisier HERFD Kβ pre-edges (Fig. 4). Fig. 5b shows calculated Fe K α centroids as a function of Fe³⁺/ Σ Fe ratios for the same garnets. The correlation between Fe K α centroids and garnet Fe³⁺/ Σ Fe ratios is improved relative to the HERFD Fe $K\beta$ centroids, but neither centroidbased calibration matches the resolution of the I-ratio or $E_{0.9}$ methods. This finding is consistent with the previous observations of Berry et al., 2010 and Dyar et al., 2012. We note that both the $K\alpha$ and $K\beta$ centroids of the eclogitic garnets appear to plot along the same trendline as the peridotitic garnets, which indicates the poorer correlations between preedge centroid energies and $\mathrm{Fe}^{3+}/\Sigma\mathrm{Fe}$ ratios do not result from differences in garnet composition or crystal structure (Dyar et al., 2012). At present, HERFD Fe KB XANES does not yield a higher resolution parameterization for garnet $Fe^{3+}/\Sigma Fe$ ratios compared to conventional

The $E_{0.9}$ method is our preferred parameterization for application to garnet unknowns because it is less sensitive to garnet composition in spectra that have been corrected for the effects of over-absorption. We apply the "low ferric" calibration to predict the $Fe^{3+}/\Sigma Fe$ ratios of four eclogitic garnets from the Slave Craton (Kopylova et al., 2016) with known $Fe^{3+}/\Sigma Fe$ ratios from Mössbauer spectroscopy that are not part of our XANES calibration. We find that our low ferric calibration returns $Fe^{3+}/\Sigma Fe$ ratios on the Slave Craton garnets within the calibration uncertainty of ± 0.02 (Fig. 6).

5.2. Flank method

We compare the $Fe^{3+}/\Sigma Fe$ ratios of garnet reference materials measured by the flank method with those measured by Mössbauer spectroscopy in Fig. 7 and Table 4. Each data point in Fig. 7 is the mean of up to 25 individual flank method measurements on each garnet reference material. Overall, there is an excellent correlation between the results of the two techniques. The 80 nA flank method analyses appear to match the $Fe^{3+}/\Sigma Fe$ ratios determined by Mössbauer slightly better compared to the 60 nA flank method analyses, and with lower standard deviations, despite the abbreviated number of analyses included in the 80 nA calibration compared to the 60 nA calibration. Höfer and Brey (2007) estimate that the uncertainty of the flank method may be as low as ± 0.02 –0.04 $Fe^{3+}/\Sigma Fe$ with repeated measurements on homogeneous reference materials.

6. Comparison of XANES and flank method for determining the ${\rm Fe}^{3+}/\Sigma{\rm Fe}$ ratios of garnet

Both XANES and the flank method may be used to determine the ${\rm Fe}^{3+}/\Sigma{\rm Fe}$ ratios of garnets with high spatial and analytical resolution, but each method has distinct advantages. The major advantage of the flank method over XANES is instrument accessibility. Electron microprobes are commonly available at many institutions, while synchrotron user facility beamlines capable of high resolution XANES with a focused spot are not. Analytical time at synchrotrons is often awarded based on scores from competitive peer-reviewed proposals, further limiting user access.

The disadvantage of the flank method is that any single flank method measurement is less precise than any single XANES analysis by greater than a factor of four, thus requiring substantially more analytical time. Höfer and Brey (2007) recommended reporting the Fe³⁺/ Σ Fe ratios of garnets as the mean of 25 analyses on each sample or grain. Each individual analysis will require up to 10 min if Fe L β and L α peaks are analyzed on a single spectrometer, yielding a total analytical time of ~250 min/reported Fe³⁺/ Σ Fe ratio. The averaging of many measurements is critical for obtaining accurate garnet Fe³⁺/ Σ Fe ratios with the

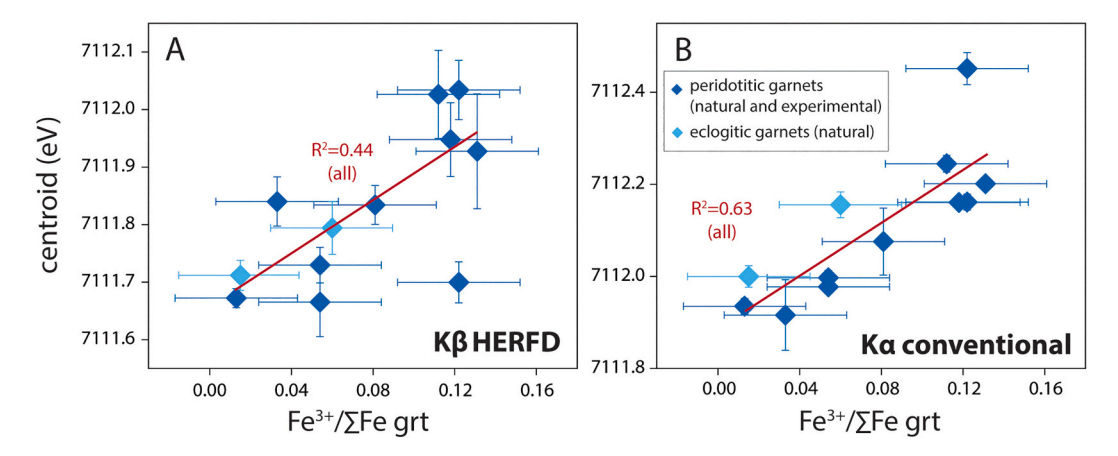


Fig. 5. Fe-XANES centroids plotted as a function of Mössbauer-determined $Fe^{3+}/\Sigma Fe$ ratios for select garnets. A) The correlation between calculated HERFD Fe Kβ centroids and $Fe^{3+}/\Sigma Fe$ ratios for garnets with $Fe^{3+}/\Sigma Fe$ from 0.013 to 0.13 is poor ($Fe^{2}=0.44$) compared to Fe Kα I-ratio and Fe^{2} 0.2 calibrations. B) Conventional Fe Kα centroids are better correlated ($Fe^{2}=0.63$) with $Fe^{3+}/\Sigma Fe$ ratios for the same garnets shown in panel A. However, neither centroid-based garnet XANES calibration matches the resolution of either I-ratio and Fe^{2} 0. calibrations. Vertical error bars are the standard errors of centroid fits (panel A) or standard deviations of up to 24 centroid fits (panel B); horizontal errors bars represent estimated Mössbauer spectroscopy errors of Fe^{2} 1.

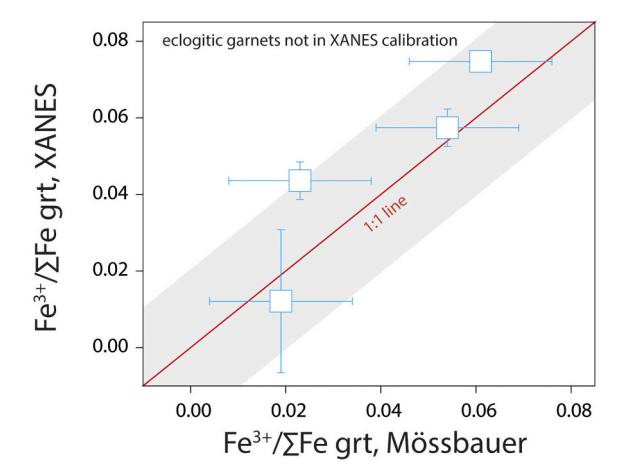


Fig. 6. Fe³⁺/ Σ Fe ratios calculated from the energy position of the Fe-edge at 90% normalized intensity (E_{0.9} low ferric calibration) compared to Mössbauer measurements for garnets in eclogitic xenoliths from the Slave craton (Kopylova et al., 2016). Vertical error bars are the standard deviations of XANES analyses. Horizontal error bars are the standard errors of Mössbauer measurements reported by Kopylova et al. (2016). The gray shaded region shows the calculated uncertainty (Fe³⁺/ Σ Fe = \pm 0.02) of the E_{0.9} low ferric XANES calibration.

flank method because any individual analysis may deviate significantly from the mean.

Fig. 8 shows the calculated Fe³⁺/ Σ Fe ratios for 25 individual Flankmethod analyses of garnet reference materials measured at 60 nA compared to garnet $Fe^{3+}/\Sigma Fe$ ratios measured by Mössbauer spectroscopy. The total range of the individual $\mbox{Fe}^{3+}/\Sigma\mbox{Fe}$ ratios calculated from the Flank-method at 60 nA extends up to five or six times the mean value of the sample within a single analytical session (e.g., calculated flank method $Fe^{3+}/\Sigma Fe$ ratios for HRV247A at 60 nA range from -0.04 to 0.07; the mean of n = 25 analyses in this session is $Fe^{3+}/\Sigma Fe = 0.02$; Supplement). The total range of the individual $Fe^{3+}/\Sigma Fe$ ratios calculated from XANES spectra across all sessions tends to be much lower (e. g., calculated XANES $\mathrm{Fe}^{3+}/\Sigma\mathrm{Fe}$ ratios for HRV247A range from 0 to 0.03; the mean of n = 20 analyses across three analytical sessions is $Fe^{3+}/\Sigma Fe = 0.02$; Supplement). While the flank method and XANES vield the same mean $Fe^{3+}/\Sigma Fe$ ratio for garnet HRV247A, any individual flank method analysis is considerably less precise than any individual XANES analysis. The precision of each method is compared in Fig. 9, which illustrates how the standard error (SE) of each method shifts as a

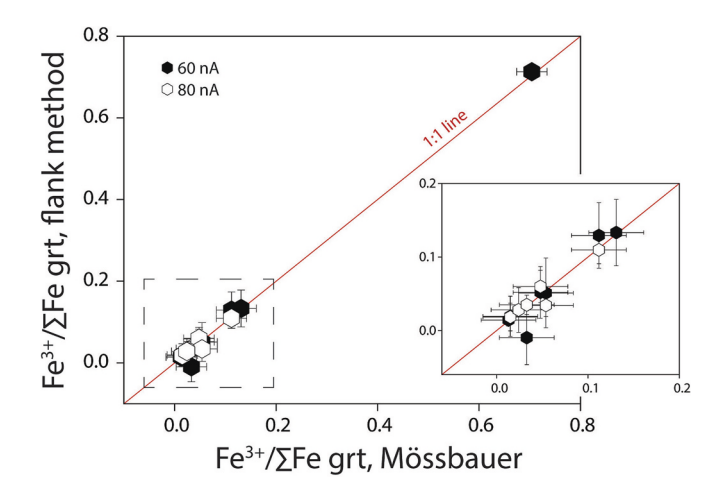


Fig. 7. Comparison of mean $Fe^{3+}/\Sigma Fe$ ratios of garnet reference materials calculated from the flank method and measured by Mössbauer spectroscopy. Data aer shown for flank method measurements performed at 15 kV, 60 nA and 15 kV, 80 nA. The inset image shows a magnified view of garnets with low $Fe^{3+}/\Sigma Fe$ ratios. Vertical error bars are the standard deviations of up to 25 flank method measurements. Horizontal error bars are estimated Mössbauer spectroscopy errors of \pm 3% $Fe^{3+}/\Sigma Fe$.

function of analysis number (n) for two garnet reference materials. Standard error was calculated as

$$SE = SD/\sqrt{n} \tag{1}$$

where SD is the standard deviation of all analyses. Fig. 9 shows the standard error of flank method analyses for PHN5267 (60 nA) and HRV247A (60 nA and 80 nA) and all XANES analyses for HRV247A. The precision of XANES is higher (i.e., the SE is lower) than all flank method approaches, regardless of the beam current or number of analyses taken. The data in Fig. 9 suggest that beyond ~ 10 flank method analyses there are only limited improvements in the precision of the method. This result is supported by Hezel et al. (2024), who find that the mean of 9 to 16 flank method analyses per sample yields the same result as the mean of 25 analyses per sample. Consequently, flank method measurement time per sample may be greatly reduced relative to the original recommendation of Höfer and Brey (2007) of 25 spots per sample.

It is not obvious why the SE of the 60 nA flank method measurements of PHN5267 are greater than the SE of flank method measurements of

Table 4
Comparison of Fe³⁺/ \sum Fe ratios for select garnet reference materials measured by Mössbauer spectroscopy, conventional Fe K α XANES (E_{0.9} calibrations) and the flank method.

	Flank method				Fe Kα XANES (E _{0.9})		Mössbauer		
Sample	n	Current	Predicted Fe ³⁺ /∑Fe	SD	Predicted Fe ³⁺ /∑Fe	Calibration uncertainty	Fe ³⁺ /∑Fe	Estimated SE	
HRV247a	24	60.0	0.02	0.03	0.02	0.02	0.02	0.03	
PHN5267	25	61.8	0.13	0.05	0.13	0.02	0.13	0.03	
BD2501	25	61.6	0.13	0.04	0.12	0.02	0.11	0.03	
PHN1917	25	62.1	0.05	0.04	0.04	0.02	0.05	0.03	
FRB838	25	61.6	-0.01	0.04	0.04	0.02	0.03	0.03	
PHN5549	25	62.9	0.05	0.05	0.07	0.02	0.05	0.03	
AW14	25	59.5	0.01	0.01	0.02	0.02	0.01	0.03	
AW52a	25	59.9	0.71	0.01	0.86	0.02	0.70	0.03	
FRB838	4	80.0	0.04	0.01	0.04	0.02	0.03	0.03	
PHN5549	4	79.5	0.03	0.01	0.07	0.02	0.05	0.03	
DE15	25	78.4	0.03	0.03	0.03	0.02	0.02	0.03	
HRV247A	25	77.5	0.02	0.02	0.02	0.02	0.02	0.03	
BD2501	5	77.0	0.11	0.02	0.12	0.02	0.11	0.03	
PHN1917	5	76.9	0.06	0.02	0.04	0.02	0.05	0.03	

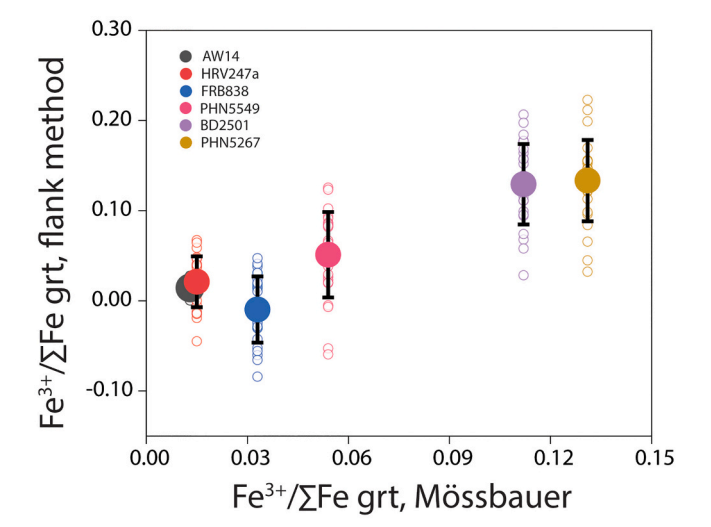


Fig. 8. Comparison of $\mathrm{Fe^{3+}/\Sigma Fe}$ ratios of select garnet reference materials calculated from the flank method and measured by Mössbauer spectroscopy. Data are shown for flank method measurements performed at 15 kV, 60 nA. The mean of 25 individual flank method analyses on each garnet is represented by the large, filled-in circles. Black bars represent the standard deviation of the mean of 25 analyses. The open circles represent calculated $\mathrm{Fe^{3+}/\Sigma Fe}$ ratios for individual flank method analyses included in the mean.

HRV247A at equivalent beam current. The higher standard deviation of the PHN5267 analyses could be due to heterogeneity in the garnet reference material. However, n = 13 XANES analyses of PHN5267 have $SD = 0.01 \text{ Fe}^{3+}/\Sigma \text{Fe}$ across all beam sessions, which suggests sample heterogeneity is not the cause of the high SE of the flank method analyses of this garnet. We note that the electron microprobe beam conditions were less reproducible during the 60 nA flank analyses of PHN5267 compared to the 60 nA analyses of HRV247A. The beam current for n =24 60 nA analyses of HRV247A has SD = 0.08 nA, while the beam current for n = 25 60 nA analyses of PHN5267 has a higher standard deviation of 0.34 nA (Supplement). However, variations in beam conditions should cancel out in calculation of the L β /L α ratio. The higher SE of the PHN5267 analyses may be due to low count rates at 60 nA, and this issue may be resolved at higher beam currents (e.g., compare 60 nA and 80 nA analyses for HRV247A in Fig. 9). Our beam conditions were chosen to replicate the earlier methodologies of Höfer and Brey (2007) and Tao et al. (2018) that utilized beam currents of 60 nA. However, the more recent studies of Hezel et al. (2024) and Wang et al. (2022) both performed garnet flank method measurements at 120 nA, which should result in improved analytical precision relative to measurements

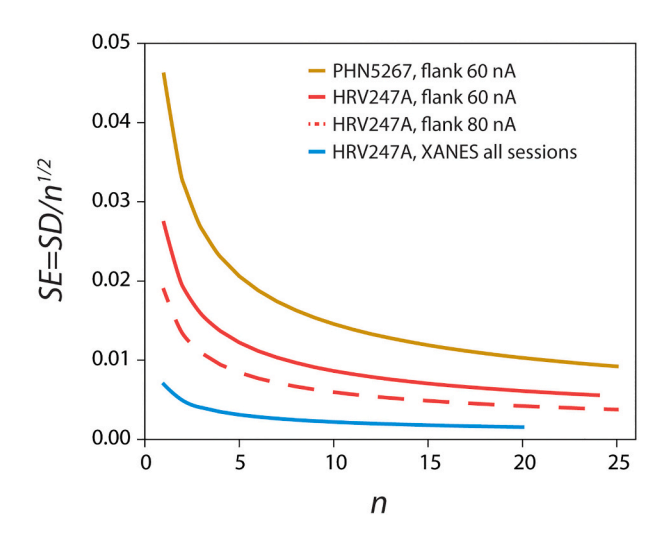


Fig. 9. Comparison of standard errors (SE) for flank method analyses of PHN5267 (60 nA) and HRV247 A (60 and 80 nA). The SE of the flank method measurements of PHN5267 at 60 nA is smaller than the estimated SE of Mössbauer spectroscopy ($\pm 0.03~{\rm Fe}^{3+}/\Sigma{\rm Fe}$) after three analyses. The SE of flank method analyses of HRV247 A do not rise above those estimated from Mössbauer at either analytical condition but we note the precision of the 80 nA measurements is greater than the 60 nA measurements. The precision of XANES analyses (blue line) is substantially higher than all flank method approaches. (For interpretation of the references to colour in this figure legend, the reader is referred to the web version of this article.)

performed at 60 or 80 nA.

We applied XANES and the flank method to measure the Fe³⁺/ΣFe ratios of experimental and natural garnets with unknown Fe³⁺/ΣFe ratios. Two garnets are from piston-cylinder experiments (Holycross and Cottrell, 2022, 2023) and four garnets are from eclogites in the Cycladic Blueschist Belt (Syros, Greece; e.g., Okrusch and Brocker, 1990; Seck et al., 1996; Dragovic et al., 2012) (Figs. S1, S2). All flank method analyses were performed at 80 nA in the same session; XANES analyses were performed in two beam sessions. All analytical procedures followed those outlined in the methods; additional details are presented in the Supplement.

At least three flank method and XANES analyses were taken on each garnet to calculate the mean and standard deviation of the analyses. Flank method traverses were performed on garnets from two eclogitic samples (JAGSY-61D, JAGSY-229 A); calculated $Fe^{3+}/\Sigma Fe$ values at each spot on the traverse represent only one flank method measurement (Supplement). We observe no meaningful variation in flank method

Fe³⁺/ Σ Fe ratios in the traverses and use all traverse Fe³⁺/ Σ Fe values to calculate an average Fe³⁺/ Σ Fe ratio for these two garnets. Garnet reference material DE15 was analyzed throughout the flank method session to monitor for potential drift over time, but no systematic drift in calculated Fe³⁺/ Σ Fe ratio was observed. Fe³⁺/ Σ Fe ratios of experimental and natural garnets measured by XANES range from 0.03 to 0.11, while five of the six Fe³⁺/ Σ Fe ratios calculated from the average of n=3+ Flank-method measurements record Fe³⁺/ Σ Fe =0.08 (Supplement). The offset between garnet Fe³⁺/ Σ Fe ratios calculated with XANES and the flank method may result from the relative precision of each methodology. This finding highlights the need to average many individual flank method analyses to obtain accurate garnet Fe³⁺/ Σ Fe ratios with this technique.

7. Implications

The $Fe^{3+}/\Sigma Fe$ ratios of garnets may reflect the redox state of Earth's interior and are consequently of major interest to petrologists. Iron XANES and the flank method for electron microprobe offer the possibility of characterizing garnet $Fe^{3+}/\Sigma Fe$ ratios with high spatial and analytical resolution, provided the development of appropriate calibrations with standards that have well known Fe³⁺/ Σ Fe ratios. We have demonstrated that the energy of the Fe-XANES main absorption edge at an arbitrary intensity of 0.9 (E_{0.9}) is highly sensitive to garnet Fe³⁺/ Σ Fe ratios and insensitive to garnet composition when the effects of selfabsorption have been accounted for. The E_{0.9} parameterizations produced here may be used to characterize the $Fe^{3+}/\Sigma Fe$ ratios of garnet unknowns with an uncertainty of $\pm 0.02 \, \text{Fe}^{3+}/\Sigma \text{Fe}$. The high precision of our calibration is critical for accurate measurement of peridotitic and eclogitic garnets with low $Fe^{3+}/\Sigma Fe$ ratios. Garnet reference materials from Table 1 have been prepared and mounted in a two one-inch rounds suitable for many analytical applications. Garnet reference materials detailed in Luth et al., 1990 and Canil and O'Neill (1996) (Table 1) are available for loan as a single mount as NMNH Catalog # 118530. Garnet reference materials E2, L78, E1, UHP666, PC287b and PC288a (Table 1) are available for loan as a separate single mount as NMNH Catalog # 118540. Loan requests may be made to the Department of Mineral Sciences at the National Museum of Natural History, Smithsonian Institution.

CRediT authorship contribution statement

Megan Holycross: Conceptualization, Formal analysis, Funding acquisition, Investigation, Methodology, Writing – original draft, Writing – review & editing. Elizabeth Cottrell: Conceptualization, Formal analysis, Methodology, Supervision, Writing – review & editing. Jay Ague: Conceptualization, Funding acquisition, Writing – review & editing. Antonio Lanzirotti: Formal analysis, Methodology, Writing – review & editing. Matthew Newville: Formal analysis, Methodology, Writing – review & editing.

Declaration of competing interest

The authors declare that they have no known competing financial interests or personal relationships that could have appeared to influence the work reported in this paper.

Data availability

All data collected in support of this manuscript are available in the supplement.

Acknowledgements

We thank T. Gooding and T. Rose for lab support and E. Bullock for help with flank method analyses. Many thanks to A. Woodland and M.

Kopylova for loaned garnet samples. R. Tappero provided beamline assistance at NSLS-II. We are grateful to L. Hale, C. Brown and C. Hearn for their assistance with reference materials borrowed from the National Rock Collection at the Smithsonian. We thank T. Gooding for preparation of garnet reference materials mount (Catalog # 118530 and 118540). This manuscript was improved following constructive reviews from D. Hezel and D. Neave and comments from the editor S. Aulbach. We acknowledge funding from NSF grants EAR 1855208 (MH), EAR 0105927 (JJA) and EAR 1650329 (JJA). Portions of this work were performed at GeoSoilEnviroCARS (The University of Chicago, Sector 13), Advanced Photon Source (APS), Argonne National Laboratory. GeoSoilEnviroCARS is supported by the National Science Foundation -Earth Sciences (EAR - 1634415). This research used resources of the Advanced Photon Source, a U.S. Department of Energy (DOE) Office of Science User Facility operated for the DOE Office of Science by Argonne National Laboratory under Contract No. DE-AC02-06CH11357. Resources of the National Synchrotron Light Source II, a U.S. Department of Energy (DOE) Office of Science User Facility at Brookhaven National Laboratory, were supported under Contract No. DE-SC0012704.

Appendix A. Supplementary data

Supplementary data to this article can be found online at https://doi.org/10.1016/j.chemgeo.2024.121937.

References

- Arlot, S., Celisse, A., 2010. A survey of cross-validation procedures for model selection. Statistical Surv. 4, 40–79.
- Aulbach, S., Woodland, A.B., Vasilyev, P., Galvez, M.E., Viljoen, K.S., 2017. Effects of low-pressure igneous processes and subduction on Fe3+/EFe and redox state of mantle eclogites from Lace (Kaapvaal craton). Earth Planet. Sci. Lett. 474, 283–295.
- Bajt, S., Sutton, S.R., Delaney, J.S., 1994. X-ray microprobe analysis of iron oxidation staets in silicates and oxides using X-ray absorption near edge structure (XANES). Geochim. Cosmochim. Acta 58, 5209–5214.
- Bauer, M., 2014. HERFD-XAS and valence-to-core-XES: new tools to push the limits in research with hard X-rays? Phys. Chem. Chem. Phys. 16, 13827–13837.
- Berry, A.J., O'Neill, H.S., Jayasuriya, K.D., Campbell, S.J., Foran, G.J., 2003. XANES calibrations for the oxidation state of iron in a silicate glass. Am. Mineral. 88, 967–977.
- Berry, A.J., Yaxley, G.M., Woodland, A.B., Foran, G.J., 2010. A XANES calibration for determining the oxidation state of iron in mantle garnet. Chem. Geol. 278, 31–37.
- Berry, A.J., Stewart, G.A., O'Neill, H.S.C., Mallmann, G., Mosselmans, J.F.W., 2018. A reassessment of the oxidation state of iron in MORB glasses. Earth Planet. Sci. Lett. 483, 114–123.
- Boffa Ballaran, T., Woodland, A.B., 2006. Local structure of ferric iron-bearing garnets deduced by IR-spectroscopy. Chem. Geol. 225, 360–372.
- Bordrage, A., Balan, E., de Villiers, J.P., Cromarty, R., Juhin, A., Carvallo, C., Calas, G., Raju, P.S., Glatzel, P., 2011. V oxidation state in Fe-Ti oxides by high-energy resolution fluorescence-detected X-ray absorption spectroscopy. Phys. Chem. Miner. 38, 449–458.
- Canil, D., O'Neill, H.S.C., 1996. Distribution of ferric iron in some upper-mantle assemblages. J. Petrol. 37, 609–635.
- Cottrell, E., Kelley, K.A., Lanzirotti, A., Fischer, R.A., 2009. High-precision determination of iron oxidation state in silicate glasses using XANES. Chem. Geol. 268, 167–179.
- Cottrell, E., Lanzirotti, A., Mysen, B., Birner, S., Kelley, K.A., Botcharnikov, R., Davis, F. A., Newville, M., 2018. A Mossbauer-based XANES calibration for hydrous basalt glasses reveals radiation-induced oxidation of Fe. Am. Mineral. 103, 489–501.
- Dragovic, B., Samanta, L.M., Baxter, E.F., Selverstone, J., 2012. Using garnet to constrain the duration and rate of water-releasing metamorphic reactions during subduction: an example from Sifnos, Greece. Chem. Geol. 314, 9–22.
- Dyar, M.D., Breves, E.A., Emerson, E., Bell, S.W., Nelms, M., Ozanne, M.V., Peel, S.E., Carmosino, M.L., Tucker, J.M., Gunter, M.E., Delaney, J.S., 2012. Accurate determination of ferric iron in garnet by bulk Mossbauer spectroscopy and synchrotron micro-XANES. Am. Mineral. 97, 1726–1740.
- Dyar, M.D., Breves, E.A., Gunter, M.E., Lanzirotti, A., Tucker, J.M., Carey, C.J., Peel, S.E., Brown, E.B., Oberti, R., Lerotic, M., Delaney, J.S., 2016a. Use of multivariate analysis for synchrotron micro-XANES analysis of iron valence state in amphiboles. Am. Mineral. 101. 1171–1189.
- Dyar, M.D., McCanta, M., Breves, E., Carey, C.J., Lanzirotti, A., 2016b. Accurate predictions of iron redox state in silicate glasses: a multivariate approach using X-ray absorption spectroscopy. Am. Mineral. 101, 744–747.
- Dyar, M.D., McCanta, M., Lanzirotti, A., Steven, C.J., Ytsma, C., 2023. Calibration for iron redox state and oxygen fugacity in silicate glasses from x-ray absorption spectroscopy. Chem. Geol. 635, 121605.
- Farges, F., Brown Jr., G.E., Rehr, J.J. 1996. Coordination chemistry of Ti (IV) in silicate glasses and melts: 1. XAFS study of titanium coordination in oxide model compounds. Geochim. Cosmochim. Acta 60, 3023-3038.

- Glatzel, P., Sikora, M., Smolentsev, G., Fernández-García, M., 2009. Hard X-ray photonin photon-out spectroscopy. Catal. Today 145, 294–299.
- Gudmundsson, G., Wood, B.J., 1995. Experimental tests of garnet peridotite oxygen barometry. Contrib. Mineral. Petrol. 119, 56–67.
- Henderson, G.S., De Groot, F.M., Moulton, B.J., 2014. X-ray absorption near-edge structure (XANES) spectroscopy. Rev. Mineral. Geochem. 78, 75–138.
- Hezel, D.C., Höfer, H.E., Fichtner, A., 2024. A fast open data reduction workflow for the electron microprobe flank method to determine Fe³⁺/∑Fe contents in minerals. Am. Mineral. (in press).
- Höfer, H.E., Brey, G.P., 2007. The iron oxidation state of garnet by electron microprobe: its determination with the flank method combined with major-element analysis. Am. Mineral. 92, 873–885.
- Höfer, H.E., Weinbruch, S., McCammon, C.A., Brey, G.P., 2000. Comparison of two electron probe microanalysis techniques to determine ferric iron in synthetic wustite samples. Eur. J. Mineral. 12, 63–71.
- Holycross, M., Cottrell, E., 2022. Experimental quantification of vanadium partitioning between eclogitic minerals (garnet, clinopyroxene, rutile) and silicate melt as a function of temperature and oxygen fugacity. Contrib. Mineral. Petrol. 177, 1–23.
- Holycross, M., Cottrell, E., 2023. Garnet crystallization does not drive oxidation at arcs. Science 380, 506–509.
- Iida, A., Noma, T., 1993. Correction of the self-absorption effect in fluorescence X-ray absorption fine structure. Jpn. J. Appl. Phys. 32, 2899–2902.
- Kopylova, M.G., Beausoleil, Y., Goncharov, A., Burgess, J., Strand, P., 2016. Spatial distribution of eclogite in the Slave cratonic mantle: the role of subduction. Tectonophysics 672, 87–103.
- Luth, R.W., Virgo, D., Boyd, F.R., Wood, B.J., 1990. Ferric iron in mantle-derived garnets: implications for thermobarometry and for the oxidation state of the mantle. Contrib. Mineral. Petrol. 104. 56–72.
- McCanta, M.C., Dyar, M.D., Rutherford, M.J., Delaney, J.S., 2004. Iron partitioning between basaltic melts and clinopyroxene as a function of oxygen fugacity. Am. Mineral. 89, 1685–1693.
- Miller, W.G., Holland, T.J., Gibson, S.A., 2016. Garnet and spinel oxybarometers: new internally consistent multi-equilibria models with applications to the oxidation state of the lithospheric mantle.
- Newville, M., 2013. Larch: an analysis package for XAFS and related spectroscopies. J. Phys. Conf. Ser. 430 (1), 012007 (IOP Publishing).
- Okrusch, M., Brocker, M., 1990. Eclogites associated with high-grade blueschists in the Cyclades archipelago, Greece: a review. Eur. J. Mineral. 2, 451–478.
- Petit, P.-E., Farges, F., Wilke, M., Sole, V.A., 2001. Determination of the iron oxidation state in Earth materials using XANES pre-edge information. J. Synchrotron Radiat. 8, 952-954
- Seck, H.A., Kötz, J., Okrusch, M., Seidel, E., Stosch, H.G., 1996. Geochemistry of a meta-ophiolite suite: an association of metagabbros, eclogites and glaucophanites on the island of Syros. Greece. Eur. J. Mineral. 8, 607–624.
- Stagno, V., Frost, D.J., McCammon, C.A., Mohseni, H., Fei, Y., 2015. The oxygen fugacity at which graphite or diamond forms from carbonate-bearing melts in eclogitic rocks. Contrib. Mineral. Petrol. 169, 1–18.
- Steven, C.J., Dyar, M.D., McCanta, M., Newville, M., Lanzirotti, A., 2022. The absorption indicatrix as an empirical model to describe anisotropy in X-ray absorption spectra of pyroxenes. Am. Mineral. 107, 654–663.

- Steven, C.J., Dyar, M.D., McCanta, M., Newville, M., Lanzirotti, A., 2023. Wave vector and field orientation dependence of Fe K pre-edge X-ray absorption features in clinopyroxenes. Am. Mineral. 108, 1754–1763.
- Sutton, S.R., Lanzirotti, A., Newville, M., Dyar, M.D., Delaney, J., 2020. Oxybarometry and valence quantification based on microscale X-ray absorption fine structure (XAFS) spectroscopy of multivalent elements. Chem. Geol. 531, 119305.
- Sutton, S.R., Rivers, M.L., Chariton, S., Eng, P.J., Lanzirotti, A., Newville, M., Officer, T., Prakapenka, V.B., Ruyu, Y.J., Stubbs, J.E., Tkachev, S., 2022. GeoSoilEnviroCARS (Sector 13) at the Advanced Photon Source: a comprehensive synchrotron radiation facility for Earth science research at ambient and extreme conditions. Phys. Chem. Miner, 49, 32.
- Tao, R., Fei, Y., Bullock, E.S., Xu, C., Zhang, L., 2018. Experimental investigation of Fe3 +-rich majoritic garnet and its effect on majorite barometer. Geochim. Cosmochim. Acta 225, 1–16.
- Wang, C., Tao, R., Walters, J.B., Höfer, H.E., Zhang, L., 2022. Favorable P-T-fO₂ conditions for abiotic CH₄ production in subducted oceanic crusts: a comparison between CH₄-bearing ultrahigh- and CO₂-bearing high pressure eclogite. Geochim. Cosmochim. Acta 336, 269–290.
- Wilke, M., Farges, F., Petit, P.-E., Brown, G.E., Martin, F., 2001. Oxidation state and coordination of Fe in minerals: an Fe K-XANES spectroscopic study. Am. Mineral. 93, 235–240.
- Wilke, M., Partzsch, G.M., Bernhardt, R., Lattard, D., 2005. Determination of the iron oxidation state in basaltic glasses using XANES at the K-edge. Chem. Geol. 220, 143–161.
- Woodland, A.B., 2009. Ferric iron contents of clinopyroxene from cratonic mantle and partitioning behavior with garnet. Lithos 112, 1143–1149.
- Woodland, A.B., Koch, M., 2003. Variation in oxygen fugacity with depth in the upper mantle beneath the Kaapvaal craton, Southern Africa. Earth Planet. Sci. Lett. 214, 295–310.
- Woodland, A.B., O'Neill, H.S.C., 1993. Synthesis and stability of Fe₃²⁺Fe₃³⁺Si₃O₁₂ garnet and phase relations with Fe₃Al₂Si₃O₁₂- Fe₃²⁺Fe₃²⁺Si₃O₁₂ solutions. Am. Mineral. 78, 1002–1015.
- Woodland, A.B., O'Neill, H.S.C., 1995. Phase relations between $\text{Ca}_3\text{Fe}_2^{3+}\text{Si}_3\text{O}_{12}\text{-Fe}_2^{3+}\text{Fe}^3$ $^+_2\text{Si}_3\text{O}_{12}$ garnet and $\text{CaFeSi}_2\text{O}_6\text{-Fe}_2\text{Si}_2\text{O}_6$ pyroxene solutions. Contrib. Mineral. Petrol. 121, 87–98.
- Woodland, A.B., Seitz, H., Altherr, R., Marschall, H., Olker, B., Ludwig, T., 2002. Li abundances in eclogite minerals: a clue to a crustal or mantle origin? Contrib. Mineral. Petrol. 143, 587–601.
- Yaxley, G.M., Berry, A.J., Kamenetsky, V.S., Woodland, A.B., Golovin, A.V., 2012. An oxygen fugacity profile through the Siberian Craton—Fe K-edge XANES determinations of Fe3+/T in garnets in peridotite xenoliths from the Udachnaya East kimberlite. Lithos 140. 142-151.
- Zhang, H.L., Hirschmann, M.M., Cottrell, E., Newville, M., Lanzirotti, A., 2016. Structural environment of iron and accurate determination of Fe³⁺/∑Fe ratios in andesitic glasses by XANES and Mössbauer spectroscopy. Chem. Geol. 428, 48–58. Zhang, H.L., Cottrell, E., Solheid, P.A., Kelley, K.A., Hirschmann, M.M., 2018.
- Zhang, H.L., Cottrell, E., Solheid, P.A., Kelley, K.A., Hirschmann, M.M., 2018. Determination of Fe³⁺/∑Fe of XANES basaltic glass standards by Mössbauer spectroscopy and its application to the oxidation state of iron in MORB. Chem. Geol. 479, 166–175.